This is a repository copy of *Multiphase Large Eddy Simulation of a Pulsed Sieve-Plate Extraction Column*.

White Rose Research Online URL for this paper:
http://eprints.whiterose.ac.uk/134953/

Version: Accepted Version

Multiphase Large Eddy Simulation of a Pulsed Sieve-Plate Extraction Column

Daniel W Theobald*, Bruce Hanson, Michael Fairweather, and Peter Heggs

*School of Chemical and Process Engineering, University of Leeds, Email: pm11dt@leeds.ac.uk

ABSTRACT

Presented here is research resulting from a framework of single-phase and multiphase modelling trials. These are intended to accurately simulate the internal flow phenomena arising in pulsed sieve-plate extraction columns representative of those found in industry. Three-dimensional unsteady flow calculations using large eddy simulation coupled with dynamic sub-grid scale modelling have been used to capture the transient effects of sinusoidal flow conditions using the open source CFD code OpenFOAM®. Multiphase interface interactions are modelled using the volume of fluid method with appropriate heavy and light phase fluidic properties capturing surface tension, density and viscous effects. The system studied consists of a 150 mm diameter column with two perforated plates with a fractional free area of 25 %, operational under 1 Hz pulsing frequency at a 50 mm amplitude and plate spacing of 300 mm. The materials simulated include water (single-phase) and 3 M nitric acid and dodecane / tributyl phosphate mixture at 30 vol% (multiphase). Results are compared with appropriate correlations from literature. The dispersive mixing efficiency of the system was also evaluated via a mixing index value which allows quantification of the ratio of rotational and irrotational flow components. This study has found that the predictive methods employed are effective at capturing the different scales of turbulence present within pulsed sieve-plate extraction columns, and its influence on their operation. As such, the work highlights the ability of large eddy simulation-based modelling to predict the complex flows in such column geometries. Furthermore, the techniques employed provide valuable insight into the hydrodynamic flow characteristics and mixing mechanisms arising within pulsed sieve-plate extraction columns.

INTRODUCTION

Solvent extraction processes are dominant within current and proposed Generation IV aqueous SNF reprocessing flow sheets. Namely, pulsed sieve-plate extraction columns (PSPECs) play an integral role in facilitating the safe and effective removal of Pu, U and, potentially, transuranic (TRU) species from spent nuclear fuel (SNF) liquors for reuse in next-generation fuels [1]. Fig. 1 illustrates a schematic of a typical PSPEC used within the nuclear industry for SNF reprocessing. PSPECs are designed to provide interfacial mixing of two immiscible fluids, during counter-current flow, in order to facilitate mass transfer between phases by maximising effective mass transfer area via droplet formation. In order to achieve efficient levels of mass transfer, droplet size is minimised through the application of shear forces [2]. A pulsed light phase is introduced at the bottom of the column and a heavy phase is fed continuously at the upper end of the column. Gravitational effects from a density differential between the two fluids causes settling within the decanters at the top and bottom of the column for the light and heavy phases respectively, as well as providing the driving force for countercurrent flow [3]. Pulsation of the light phase feed causes cyclic mixing of the fluid across the stationary perforated sieve-plates resulting in shear forces leading to droplet formation [2]. Understanding the complex flow phenomena arising from the pseudo-steady state characteristics of the PSPECs is necessary for effective process design, operation, control and optimisation.

---

[a] OpenFOAM® is a registered trademark of OpenCFD Ltd licensed in perpetuity to the OpenFOAM Foundation.
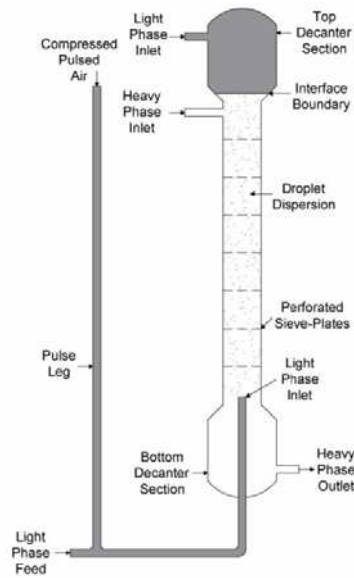
Fig. 1. Generic Industrial PSPEC Design Used in SNF Reprocessing.

From a review of available literature presented by Yadav and Patwardhan [4], it is evident that little is known about the fundamental hydrodynamic behaviour of pulsed sieve-plate extraction columns. Specifically, the physical phenomena present during operation and the roles that these effects play on the efficiency and operating characterises of these processing units. Some resurgence in PSPEC research has been made apparent over the past decade through new hydrodynamic investigations using computational fluid dynamics (CFD). However, these studies are mainly rudimentary, typically employing Reynolds-averaged Navier-Stokes (RANS) methods using k-ε turbulence modelling to close the descriptive equations [5][6][7].

This investigation moves away from time-averaged modelling approaches in order to provide the level detail that is required for a study of this nature. Through the use of time-dependent, three-dimensional, turbulent eddy-resolving methods, the flow fields at all length and time scales within such columns can be predicted, allowing a detailed analysis of their mode of operation. This is being achieved using large eddy simulation (LES) computational techniques coupled with dynamic sub-grid scale (SGS) modelling that provides accurate and reliable predictions of the complex flows in these extractions columns. The accuracy of the modelling technique employed means that comparative experimental data is not necessary for the mostly qualitative assessments made at this stage. However, a framework of experimental validation has been considered in future work.

The results presented from this investigation are of a single and multiphase PSPEC model, using boundary conditions derived from the typical throughput and operating parameters of operational reprocessing facilities. Initially, the aim is to characterise the flow characteristics, pressure drops and mixing behaviour of a simple single-phase system. Subsequently, a revised multiphase PSPEC model, using the interface capturing volume of fluid (VOF) method, is evaluated under the same criteria using modified boundary conditions. The information gained from this study will ultimately be used to develop robust and accurate methods to facilitate the design of high-efficiency columns through a further framework of mass transfer optimisation studies.

METHODOLOGY

Column Geometry and Process Conditions

The column geometry dimensions where chosen to best replicate columns found in industry, particularly within Pu processing lines within SNF reprocessing plants. PSPECs geometry dimensions are constrained as to avoid criticality events from rich Pu laden SNF liquors through a safety-by-design philosophy. As such, industrial PSPECs are typically thin, up to 0.3 m in diameter, and long, around 12 m high, with many separation stages divided by perforated sieve-plates [8]. Sieve-plates used are generally of 2 mm thickness, have a triangular pitch array of holes between 0.83 – 4.78 mm diameter giving a fractional free area of between 10 – 60 %, a free area of around 23 % is common. Additionally, plates are said to be spaced 12.5 – 100 mm apart [9]. The geometry chosen to accommodate these criteria are shown Fig. 2 and the relevant dimensions are summarised in TABLE I.
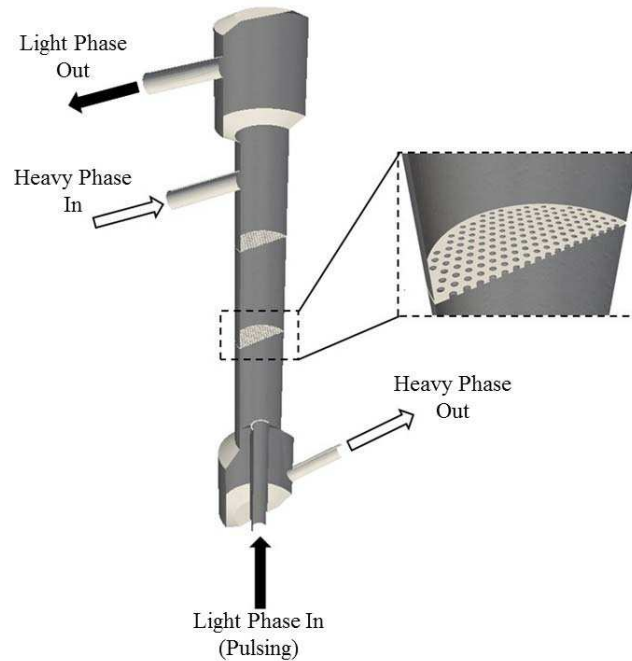

Fig. 2. Y-Symmetry Plane Isometric View of the PSPEC Geometry used in CFD Simulations.

TABLE I. Characteristic Dimensions of the PSPEC Geometry used in CFD Simulations.

Parameter	Dimension	Parameter	Dimension
Column Diameter, D (m)	150	Number of Holes, N_h	283
Hole Diameter, d (m)	4.46×10^{-3}	Number of Plates, N_p	2
Plate Spacing, h (m)	0.300	[a] Decanter Height (m)	0.300
Plate Thickness, t (m)	0.002	[a] Decanter Diameter (m)	0.250
Column Height, H (m)	1.604	Inlet / Outlet Diameters (m)	0.050
Fractional Free Area, e (%)	25	Light Phase Inlet Wall Thickness (m)	5.54×10^{-3}

[a] Both the top and bottom decanters have the same height and diameter.

The open source computer-aided design (CAD) software SALOME (version 8.3.0) was used to produce the geometry seen in Fig. 2. A column diameter of 150 mm was chosen with two plates of thickness 2 mm and a fractional free area of 25 % containing 283 holes. In the interest of computational efficiency, a two-plate

geometry was chosen on the basis that the inter-compartmental hydrodynamics remain largely unchanged past the second plate. Similar reasoning has been used for justification of 2 – 4 plate models by previous investigators [6][7][10]. The plate spacing was kept constant at 300 mm, this is larger than the mentioned recommended based on typical designs queues [10]. In subsequent optimisation work, this will be reduced in order to observe the resulting effects. The additional plate spacing will allow for review of the inter-compartmental mixing effects and jetting characteristics which, in turn, will allow for justified alteration to the spacing based on optimised mixing parameters. A reasonable decanter height and diameter was chosen to provide enough fluid volume to dissipate agitative effects and allow for settling in these regions. The inlet and outlet diameters where kept constant at a roughly 2-inch nominal pipe size (50 mm). The light phase inlet represents an ANSI schedule 80 pipe given a 2-inch nominal size, the pipe thickness protruding into the column is in-line with this specification having a thickness of 5.54 mm [11].

The boundary conditions chosen for this simulation, namely inlet velocities, are based on industrial throughputs of PUREX processing plants in the UK and France. It was assumed such a plant would require processing 25 m^3 of SNF liquor containing a U concentration of 250 gU/L in 3 M HNO$_3$. Using this design basis, the heavy (aqueous) phase volumetric throughput can be calculated. Subsequently, the organic (light) phase throughput can be determined on a simplified mass balance basis assuming a TBP concentration of 30 vol%, in dodecane, a decontamination factor of 5000 and a mass transfer efficiency of 50 %. According to McKetta [12], the total calculated throughput of the combined organic and aqueous feeds ($\sim$ 0.66 L/s) are in-line with what is expected from a column of this diameter. The volumetric throughputs calculated were converted into velocities based on the inner pipe cross-sectional area. These values were used for the multiphase model. For the single-phase model, the volumetric throughput had to first be adjusted to consider the differences in density between the chosen single-phase and multiphase fluids, particularly for the light phase inlet. This was done by keeping the mass flow constant at each inlet and adjusting for volumetric changes based on density accordingly. For the single-phase model, the inlet velocity of the heavy phase inlet was calculated to be 0.147 m s^{-1} and 0.163 m s^{-1} for the light phase inlet. For the multiphase model, the heavy phase inlet velocity was calculated to be 0.147 m s^{-1} and 0.201 m s^{-1} for the light phase inlet. In both cases, the light phase inlet was pulsed sinusoidally according to Eq. 1

$$U_{in} = Afsin(2\pi ft) + U_{offset} \qquad \text{(Eq. 1)}$$

where U_{in} is the inlet velocity, A the amplitude, f is the pulse frequency, t is the time in the pulse phase, and U_{offset} is the mean velocity offset *i.e.* the required velocity throughput calculated previously for the light phase inlet. The light phase inlet was pulsed at an amplitude of 50 mm and at a frequency of 1 Hz.

In each case, standard temperature and pressure conditions were assumed. In the single-phase model, the density of water was taken to be 1000 kg m^{-3} and the kinematic viscosity is taken to be 0.891$\times$10^{-6} m^2 s^{-1} [13]. For the multiphase model, the density of dodecane, TBP and HNO$_3$ was taken to be 750 kg m^{-3}, 973 kg m^{-3} and 1110 kg m^{-3} respectively [13]. The density of the organic phase mixture was calculated based on vol% giving a density of 806 kg m^{-3}. The values of the kinematic viscosities of dodecane, TBP and HNO$_3$ were taken to be 1.82$\times$10^{-6} m^2 s^{-1}, 3.62$\times$10^{-6} m^2 s^{-1} and 1.02 m^2 s^{-1} respectively. The kinematic viscosity of the organic phase mixture was calculated based on Eq. 2:

$$v^{1/3} = x_a v_a^{1/3} + x_b v_b^{1/3} \qquad \text{(Eq. 2)}$$

where v is kinematic viscosity, x is the mass fraction of the fluid component [14]. It was found to be 2.35$\times$10^{-6} m^2 s^{-1}. The outlet pressures were assumed to be atmospheric in both cases. A surface tension of 47.32 mN m^{-1} was used for the HNO$_3$ – TBP / dodecane system [13].

Mesh Generation

All computational simulations were carried out using the open source software OpenFOAM®. In order to produce a high-density mesh of good quality, the commercial mesh generation tool available within the CD-adapco® STAR-CCM+® environment (version 10.06.010) was chosen and meshes were converted using the OpenFOAM® pre-processing utility ccm26ToFoam. Due to the complex nature and length scales inherent to this geometry, the tetrahedral mesher was chosen to produce an unstructured three-dimensional tetrahedral mesh of 5.5 M nodes with refinement towards the plates and column walls. The available polyhedral mesher was first trialled, although once converted the OpenFOAM® mesh quality check showed poor quality in orthogonality and skewness values. This could lead to inaccuracies in the numerical operations causing the simulation to crash or diverge. These issues were not apparent upon conversion of the tetrahedral mesh. Fig. 3 shows the unstructured internal mesh used for both the single and multiphase simulations.
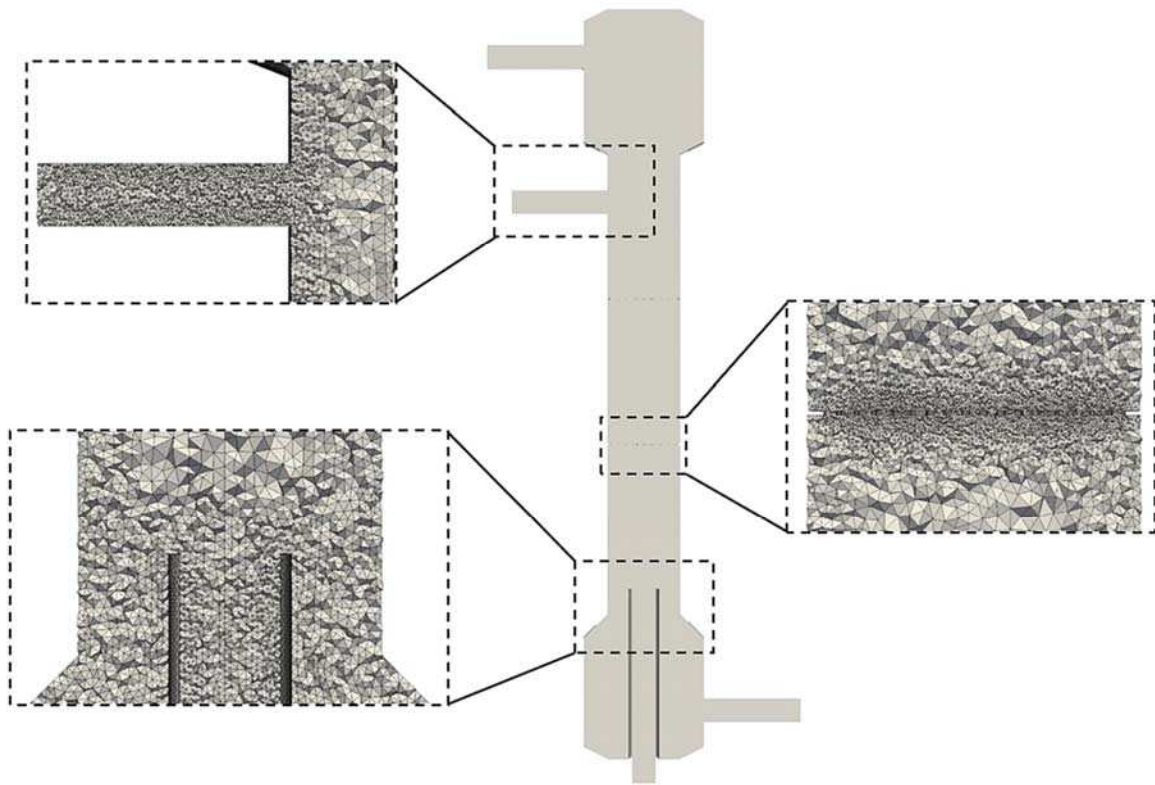

Fig. 3. Unstructured Tetrahedral Mesh Used in Both the Single and Multiphase CFD Simulations.

Single-Phase Solution Strategy

The OpenFOAM® (version 4.1) solver pimpleFoam was used in order to solve the Navier-Stokes equations using a LES approach coupled with SGS modelling via the dynamic Lagrangian model. The pimpleFoam solver is a large time-step transient solver for incompressible flows. It is based on the PIMPLE algorithm, a mixture of PISO and SIMPLE. Here inner-loop iterations (solution of all transport equations) are solved under-relaxation with additional outer-correction loops designated to iteratively solve the coupled pressure-velocity equations based on the velocity correction step, ensuring strong coupling. If the outer-correction loops are programmed for one cycle, the PIMPLE algorithm operates identically to PISO. This outer-correction step permits the use of high Courant numbers above unity with reduced risk of divergence [15]. The dynamic Lagrangian SGS model is a variation of the Smagorisnky model that uses a Lagrangian temporal-averaging approach over fluid pathlines in order to calculate SGS model coefficients based on information from the larger unfiltered energy scales. This SGS model, therefore, incorporates considerations for the turbulence history of the case, in contrast to the older and less accurate spatial averaging schemes that disregard such information. Although originally validated for systems with homogeneous directions, it is said to be readily applicable for unsteady flows with complex geometries [16].

A summary of the boundary conditions for the single-phase case are listed in TABLE III. OpenFOAM® uses a propriety list of 'boundary patch types' that are used to allocate conditions, a full list of which is defined in the OpenFOAM® user guide [17].   For the single-phase model, the inlet velocity and pressure outlet boundary conditions were specified. The heavy phase inlet, and both the heavy and light phase pressure outlets were specified as *fixedValue* according to the process conditions listed previously. In the case of the light phase inlet, the *uniformFixedValue* patch type was used which included specifications for the sinusoidal conditions required for simulating pulsed flow. The velocity outlet and pressure inlet boundary conditions were specified as *zeroGradient*. A zero velocity field condition was applied at the column walls, which includes the plates, using the patch type *noSlip*. Additional conditions for the SGS transport equations have to be stated for initialisation of the model, however, the values used for these parameters are of less consequence provided reasonable values are selected due to the nature of the solution procedure. In this case, this includes fields for the SGS turbulent viscosity and, f_{LM} and f_{MM}, scalar properties used to solve the subgrid viscosity equation [16][18].

TABLE III. Initial Boundary Conditions Used for the Single-Phase Case.

Field	Heavy Phase Inlet	Light Phase Inlet	Heavy Phase Outlet	Light Phase Outlet	Wall
Velocity	*fixedValue* (0 0 0.147)	*uniformFixedValue* *uniformValue* sine $A = 0.05$ $f = 1$ *level =* (0 0 0.163)	*ZeroGradient*	*ZeroGradient*	*noSlip*
Pressure	*ZeroGradient*	*ZeroGradient*	*fixedValue* 0	*fixedValue* 0	*fixedFluxPressure*

The discretisation used for the single-phase model were unbounded second-order upwind scheme for the velocity equations and bounded first-order upwind for the SGS model transport, this of particular importance for this SGS model as unbounded scalars can quickly lead to divergence through negative terms [18]. Convergence for the transient case was achieved when residuals fell below 1×10^{-3} for each transport equation at each time step. A time step of 1×10^{-5} s was used with an adjustable time step function; this allows the time step to be optimised automatically based on a Courant number limit. Here a limit of 5 was

used in order to take advantage of the benefits of the PIMPLE algorithm. Under-relaxation factors of 0.9 were used for the pressure field and velocity equations, and under-relaxation factors of 0.75 were used for the f_{LM} and f_{MM} equations. Under-relaxation is only used during the inner-loop iterations to improve numerical stability, the last loop being solved without under-relaxation. Four PIMPLE outer-correction loops were chosen to ensure strict time accuracy of the solution and limit the risk of divergence. Final solutions were taken when the calculations converged for at each time step, within four PIMPLE iterations. At this point, the model was run for 10 s of simulation time, and averages were taken for four points in the sinusoidal cycle for each cycle. This resulted in 4 temporally ensemble-averaged data sets averaged across 20 cycles (running at 1 Hz frequency) at phase time $t = 0$ s, $t = 0.25$ s, $t = 0.5$ s, and $t = 0.75$ s. This averaging process is visualised in Fig. 4.
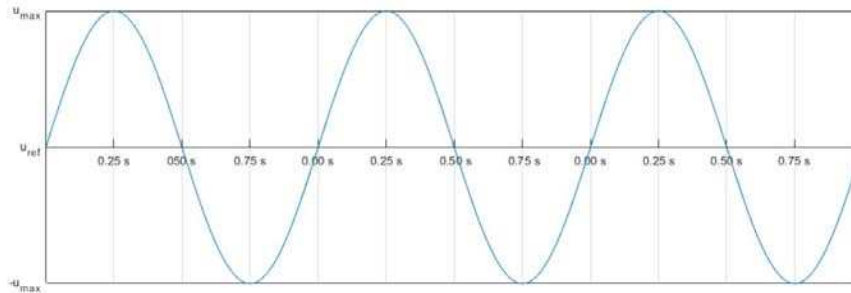

Fig. 4. Visualisation of the Temporally Ensemble-Averaged Data Sets Based on the Light Phase Inlet Velocity.

Multiphase Solution Strategy
The multiphase model was developed on the basis of the single-phase model. As before, the PIMPLE algorithm was chosen using the interface capturing VOF multi-component modelling method, executed through OpenFOAM's® interFoam solver. This multiphase modelling approach solves a single set of transport equations modelling two immiscible fluids based on a fraction function (α). This distinguishes between the two fluids using a value between zero and unity. In this case, a value of zero implies only the TBP / dodecane phase is present within the element volume. Conversely, a value of unity implies HNO_3 is present. Intermediate values represent interfaces between the two immiscible fluids [19]. The dynamic lagrangian SGS model was again used to model subgrid turbulent effects.

A summary of the boundary conditions for the multiphase case are listed in TABLE IV. For the multiphase model, the inlet velocity and pressure outlet boundary conditions were specified. Both the heavy and light phase pressure outlets were specified by *totalPressure,* here only static pressure is defined absent of dynamic pressure. This allowed for the use of the *pressureInletOutlet* velocity condition at the outlets which permits recirculation across the boundary and calculates re-entry velocity conditions based on pressure. In the case of the light phase inlet, the *uniformFixedValue* patch type was used which included specifications for the sinusoidal conditions required for simulating pulsed flow. Here, the pressure inlet boundary conditions were specified as *fixedFluxPressure* which imposes a flux that is that specified by the inlet velocity boundary condition to improve convergence. A zero velocity field condition was applied at the column walls, which includes the plates, using the patch type *noSlip*. As mentioned before, values for the SGS scalar fields were specified only to facilitate initialisation. Additionally, for this case boundary conditions for α where also specified.

TABLE IV. Initial Boundary Conditions Used for the Multiphase Case.

Field	Heavy Phase Inlet	Light Phase Inlet	Heavy Phase Outlet	Light Phase Outlet	Wall
Velocity	*fixedValue* (0 0 0.147)	*uniformFixedValue uniformValue* sine $A = 0.05$ $f = 1$ *level* = (0 0 0.249)	*pressure inletOutlet*	*pressure inletOutlet*	*noSlip*
Pressure	*fixedFluxPressure*	*fixedFluxPressure*	*total-Pressure* 0	*total-Pressure* 0	*fixedFluxPressure*
Phase Fraction	*fixedValue* 1	*fixedValue* 0	*inletOutlet*	*inletOutlet*	*zeroGradient*

The discretisation used for the multiphase model were unbounded second-order upwind scheme for the velocity equations and bounded first-order upwind for the SGS model transport terms to encourage convergence. Additionally, a first-order Gaussian linear scheme was used bounded between zero and unity for the α transport terms to enhance solver stability. Convergence for the transient case was achieved when residuals fell below 1×10^{-3} for each transport equation at each time step. A time step of 1×10^{-6} s was used with an adjustable time step function. Here a Courant number limit of 0.8 was used with, an effective interface courant number of 0.125. No under-relaxation was used in this model in order to ensure time-accurate conditions given the more transient nature of the multiphase solution. Twenty PIMPLE outer-correction loops were chosen due to the complex nature of the flow problem when not using under-relaxation, however, time steps commonly converged within two PIMPLE iterations. Final solutions were taken when time step convergence was observed and the solutions were stable.

Post-Processing and Analysis

Relevant pressure drop correlations available from literature quantitatively assesses the simulation results produced from each case. The theoretical single-phase dynamic pressure loss ΔP across the plates was calculated using the correlation given by Thornton [20], Eq. 3, and compared against data obtained during the simulation.

$$\Delta P = N_p \frac{\rho (1-e)(1-e^2)}{2C_D^2} \left(\frac{dA}{dt}\right)^2 \tag{Eq. 3}$$

Here, *dA/dt* represents the instantaneous pulse velocity, *e* is the plate fractional free area, N_p is the number of sieve-plates, and C_D is the discharge coefficient taken to be 0.6 [4]. For the multiphase case, the pressure drop due to fractional losses across the plates was estimated using the correlation given by Hafez and Baird [21], Eq. 4.

$$\Delta P = N_p \frac{\rho_c \left[1.5 - 2.5e + e^2 + \frac{1-\beta}{\beta} + \frac{0.316h}{dRe^{0.25}}\right]}{2e^2} \left(\frac{dA}{dt}\right)^2 \tag{Eq. 4}$$

$$\beta = \frac{e^2}{(1-e)(1-e^2)} \tag{Eq. 5}$$

In each case, the pressure losses were calculated and compared at t = 0.25 s corresponding to the time in the pulse cycle with the greatest pulse velocity.

In order to determine the dispersive mixing capability of the multiphase system, an additional code was written and used to calculate a mixing index λ_{MI} field during post-processing. This is a scalar value used to quantify the ratio of rotational and irrotational flow components, given by Eq. 6.

$$\lambda_{MI} = \frac{|S|}{|S|+|\Omega|} \qquad\qquad (\text{Eq. 6})$$

where $S = \frac{1}{2}[\nabla v + (\nabla v)^T]$ and $\Omega = \frac{1}{2}[\nabla v - (\nabla v)^T]$ are the rate-of-strain tensor and vorticity tensor, respectively. The mixing index, otherwise known as flow number, is commonly used in industrial colloidal applications in determine mixing effectiveness. A value of 0 represents pure rotational flow, 0.5 represents simple shear flow, and 1 represents pure elongational flow. Values towards 1 are more desirable for effective dispersive mixing [22].

RESULTS & DISCUSSION
Single-Phase

The calculated value for the total pressure loss across both sieve-plates was calculated to be 4.88 Pa. As seen in Fig. 5, the measured pressure loss from under the bottom plate (at 0.7 m) and above the second plate (at 1 m) was 4 Pa, which shows reasonable agreement with the Eq. 3. However, the correlation used can not be used to characterise the pressure drop across the column in the same way as shown in Fig. 5 which illustrates the complex pressure fluctuations within the column. Notably, the pressure spike, drop, and recovery across each plate which is particularly pronounced across the first plate. This is a consequence of Bernoulli's principle and conservation of mass across the plate, which is expected behaviour from flow over such plates [4]. This is one example wherein current PSPEC correlations fail to fully describe the complex flow behaviour therein.
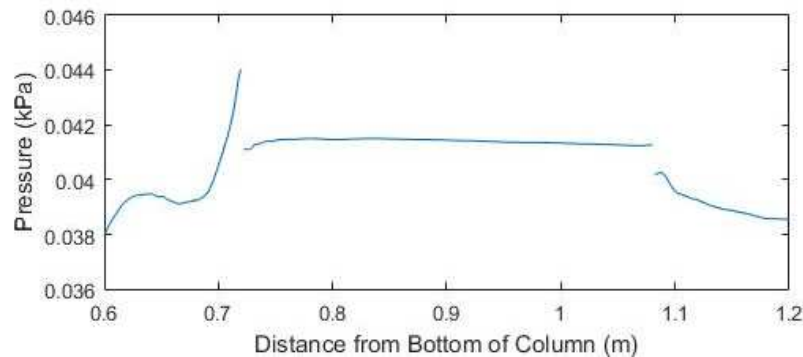

Fig. 5. Pressure Plot across two Plates in the Y-Symmetry Plane for the Single-Phase Case at t = 0.25 s.

As a way of visualising the flow patterns within the PSPEC models, a surface line integral convolution (LIC) filter was applied over the velocity field profiles. This allows for a sense of movement within the column particularly for visualising eddy structures. As shown in Fig. 6, a large amount of detail is available as a consequence of using an LES modelling methodology which has not been documented in previous studies. It is in this finer detail were comments on the design practices in these industrial columns can be made. The top compartment exhibits large rotational bodily flows, with some material flowing into the top decanter section which, in a multiphase case, would be used to agglomerate dispersed phase fluid. This behaviour could cause complication in the start-up of these systems. Within the bottom compartment, two vortices where observed to form at t = 0.25 s due to the pulsing of the bottom inlet. Both vortices followed either side of a cap-shaped region of high-velocity flow through advection towards the bottom plate; this motion is visible in Fig. 6. Although not clearly visible, jetting was observed across the centre region of the

bottom plate, to a distance roughly equal to the pulse amplitude, from the cap of high-velocity flow. In this case, the whole plate was not utilised for dispersion presumably because of wall-bounded downward flowing fluid from the top inlet.

In regards to time-varying flow characteristics, it was found that little changed through the pulse cycle apart from that mentioned in the bottom compartment and across the bottom plate. It was also apparent that the pulse amplitude used did not affect much within the centre compartment, although the value used was within the recommended pulse velocity range [9]. This suggests a lower frequency and higher amplitude should be used, closer to that of the plate spacing in order to optimise the effects of pulsing.

UMean (m/s)

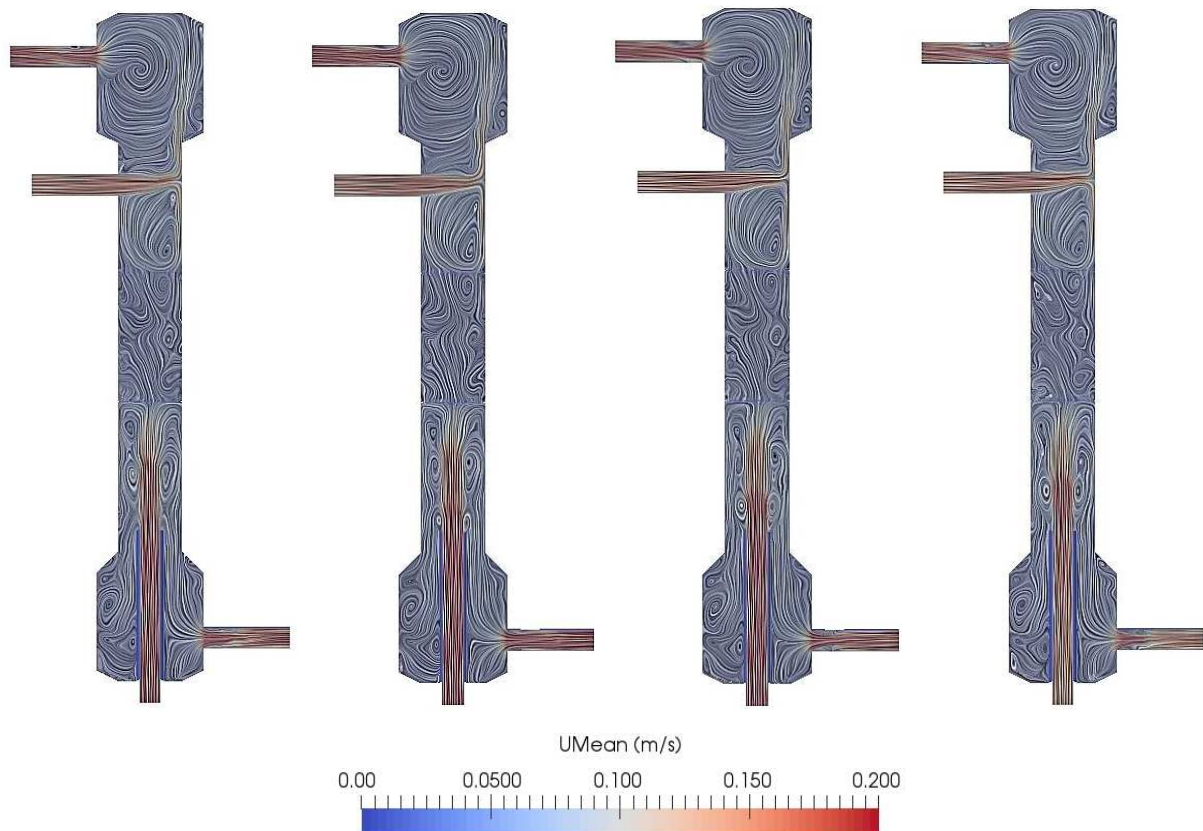0.00   0.0500   0.100   0.150   0.200

Fig. 6. Ensemble-Averaged Velocity Field Profiles Within the - PSPEC, Visualised with a Surface LIC Filter at times 0 s, 0.25 s, 0.5 s, and 0.75s from Left to Right Respectively.

Multiphase

Data regarding the pressure loss across the multiphase column were collected and plotted in Fig. 7. In contrast to the single-phase case, the multiphase case displays the characteristic pressure, spike, drop and recovery at each plate, as well as a comparatively low total pressure drop across the column in the bulk flow compared to across the plate. The measured value of the column pressure loss was taken from the spike under the bottom plate to the recovered value on top of the second plate and was found to be roughly 310 Pa. The pressure loss across one plate was calculated to be 3 Pa using Eq. 4 for two plates ($Np = 2$) and using an estimated value of $Re = 210$ based on the dispersed phase material properties and average inlet flow rate adjusted at the plates based on conservation of mass. Clearly there is a large disparity in the value observed and the values predicted from the correlation. One postulation is that the (dA/dt) term Eq. 4 is not scalable to the pulse velocities used in this investigation (> 0.1), another example of how current understanding of pulse columns fails to describe their complex behaviour.
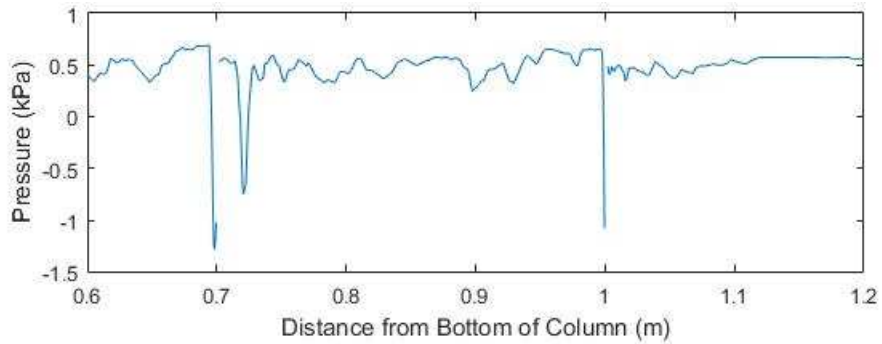
Fig. 7. Pressure Plot across two Plates in the Y-Symmetry Plane for the multiphase Case at t = 0.25 s.

The isolated dispersed phase fluid was visualised using an iso-surface filter to capture the hold-up present within the PSPEC, shown in Fig. 8. As with the single-phase case, the velocity profiles were also plotted over a surface LIC filter in order to capture the flow stream data. It was observed that in areas of dispersed phase flow there were occurrences of higher velocity flow. This could be a consequence of the reduced density in these areas. However, the velocity changes observed were much higher than expected from this alone, some areas showing velocity magnitudes six factors higher than the surrounding continues phase fluid. This suggests heavy re-circulation within the dispersed phase fluid droplets which will have an effect on mass transfer in operating pulse columns.

As with the single-phase model, the bottom compartment showed occurrences of eddy formation from the pulsing inlet that moved towards the plate via advection, but in this case through a more turbulent body of fluid. Furthermore, the stresses applied during back-stroke at t = 0.75 s appears to disrupt these eddy structures. This behaviour is illustrated in Fig. 9. The violent nature of the flow observed in the bottom compartment appears to provide adequate mixing of the dispersed phase, as shown in Fig. 8. This allows for good coverage across the sieve plate, although not ideal as there seems to be a bias flow towards the centre holes.

Fig. 8. Iso-surface of α Showing the Isolated Dispersed Phase Fluid at times 0 s, 0.25 s, 0.5 s, and 0.75s from Left to Right Respectively.
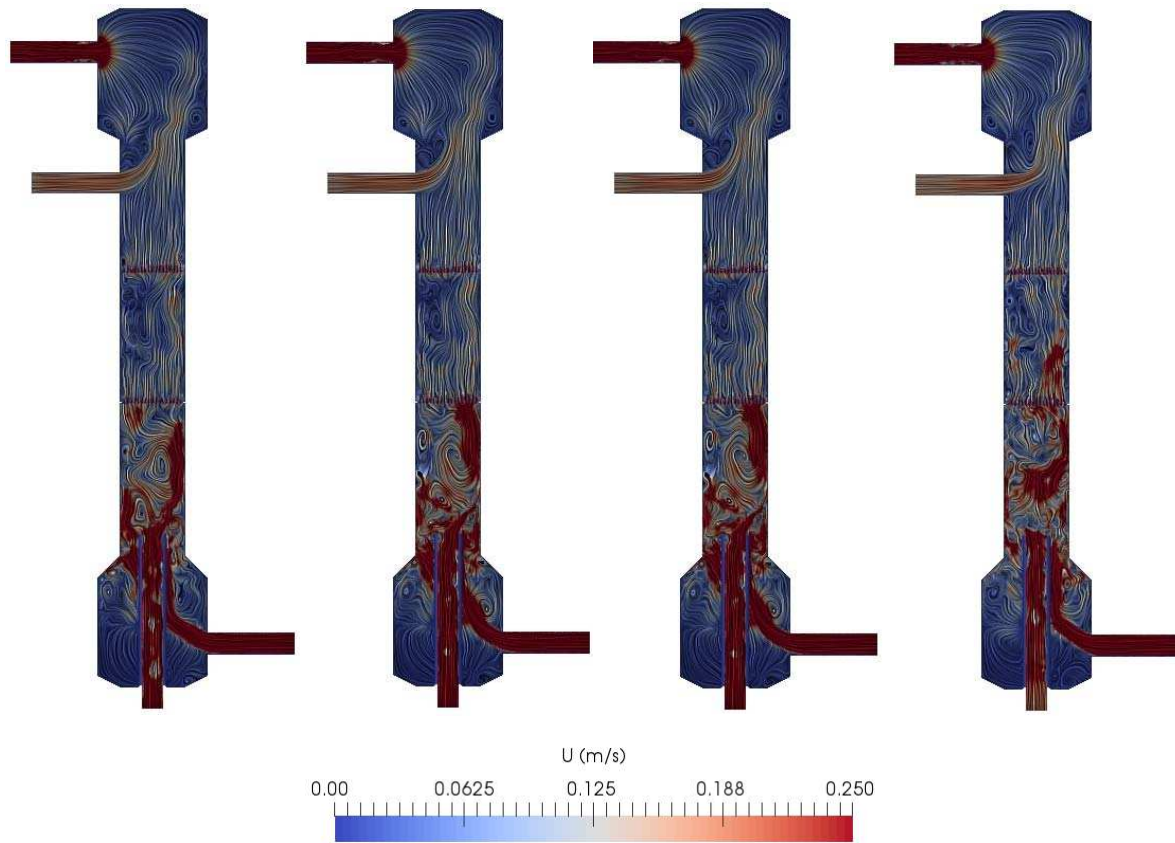
Fig. 9. Velocity Field Profiles Within the Multiphase PSPEC, Visualised with a Surface LIC Filter at times 0 s, 0.25 s, 0.5 s, and 0.75s from Left to Right Respectively.

The jetting characteristics of flow through the sieve plate holes and a clearer visualisation of the velocity profiles within the centre compartment is seen in Fig. 10. Fig. 11 is a plot of the mixing index field for the same section of the column, areas of no colour show value below a $\lambda_{MI} = 0.5$ threshold where mixing performance is deemed poor. Interestingly, the jetting behaviour across the sieve-plate appears to stay comparatively constant through the duration of the pulse cycle, only changing due to regions of higher velocity dispersed phase fluid crossing the plates. It is observed from Fig. 10 that the jets only extend to roughly a 10th of the length of the plate spacing used in this simulation. The jetting flow appears to disperse into the bulk flow thereafter. This suggests the plate spacing used here can be drastically reduced, assuming the primary mode of dispersive mixing is from shear effects at the plate and subsequent jetting phenomena. As shown in Fig. 11, the highest mixing index values are observed close the plate holes. Some strong regions of mixing are shown in the upper half of the centre compartment but are coupled with adjacent regions of poor mixing. In general, the majority of the flow domain shows fairly tolerable mixing performance, but it tends towards the lower end of values of $\lambda_{MI} = 0.5$ indicting preference towards shear flow. The use of high amplitudes or pulse frequencies could induce greater levels of elongational flow to improve dispersive mixing. This hypothesis will be studied in a future framework optimisation studies.
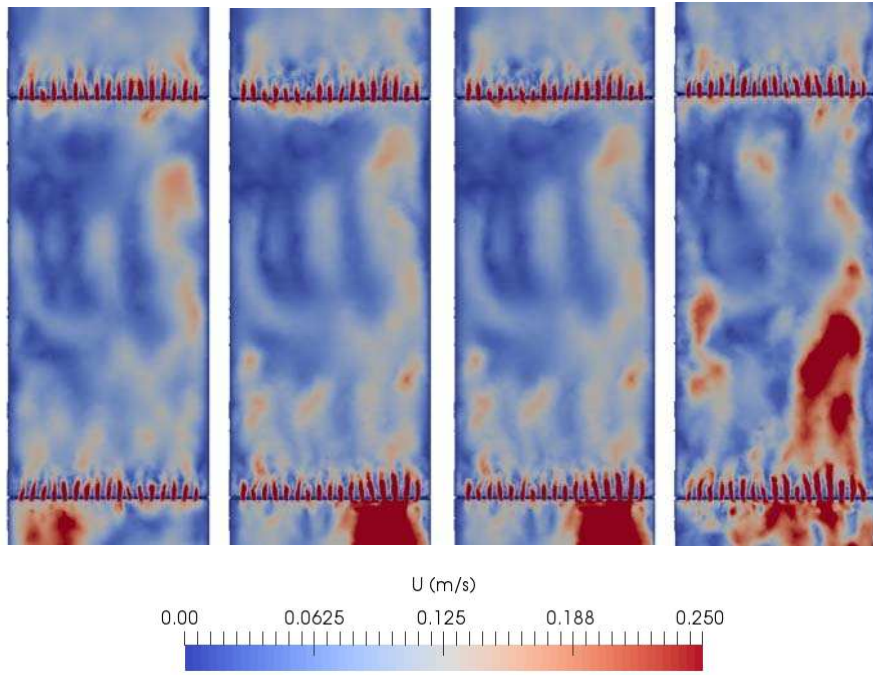
U (m/s)

0.00   0.0625   0.125   0.188   0.250

Fig. 10. Velocity Field Profile across the Centre Compartment and Two Sieve Plates Showing Jetting through Sieve holes.

Mixing Index

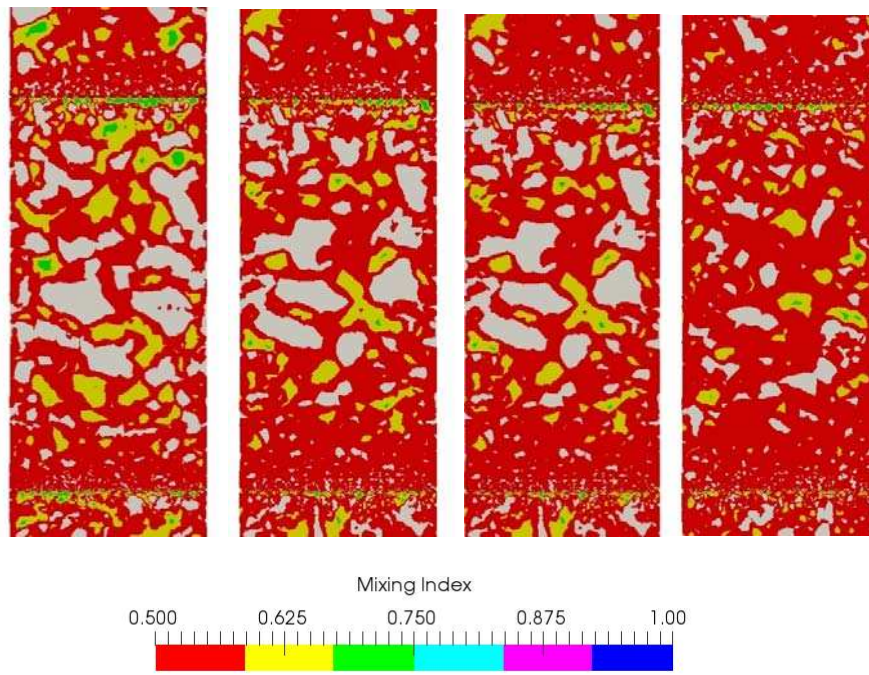0.500   0.625   0.750   0.875   1.00

Fig. 11. Mixing Index Field Profile across the Centre Compartment and Two Sieve-Plates.

CONCLUSIONS

This investigation has utilised advanced eddy resolving time-dependent three-dimensional CFD models in order to provide a deeper insight into the hydrodynamics occurring in PSPECs. Previous investigations within this area have failed to provide the level detail produced by this modelling methodology. The single-phase model showed good agreement within available pressure loss correlations from literature, whereas the multiphase model did not, potentially due to the pulse velocities used. The turbulent nature of the pulsing inlet within the bottom compartment was observed in both the single and multiphase model within eddies forming at the inlet moving towards the plate via advection. This violent behaviour showed to provide adequate dispersion of the dispersed phase fluid within the bottom compartment in the multiphase model.

The mixing performance of the multiphase model was assessed using a mixing index number derived the velocity field. Strong dispersive mixing was observed close to the sieve-plate holes. High mixing index values were observed in bulk compartmental flow, however, adjacent to regions of poor mixing. Moreover, the jetting phenomena across the sieve-plates were also observed and assessed showing poor extension into the length of the compartment. The information gained from this investigation will be used as bases in a future optimisation framework in order improve the dispersive mixing efficiencies in these industrial PSPECs. The work presented here illustrates the development of the modelling capability required for optimisation studies. Future work primarily consists of utilising more complex forms of multiphase modelling, incorporating a population balance linking to mass transfer studies. Subsequently, the knowledge gained from these simulation can be used to better improve design and operation of PSPECs which should be demonstrated in the assessment of a physical rig in a study made in parallel to this body of work.

REFERENCES

[1]   R. Taylor, "Reprocessing and Recycling of Spent Nuclear Fuel." Elsevier, Oxford, 2015.

[2]   M. Jaradat, M. Attarakih, and H. J. Bart, "Population Balance Modeling of Pulsed (Packed and Sieve-Plate) Extraction Columns: Coupled Hydrodynamic and Mass Transfer," *Ind. Eng. Chem. Res.*, vol. 50, no. 24, pp. 14121–14135, 2011.

[3]   L. E. Burkhart and R. W. Fahien, "Pulse Column Design," Ames, 1958.

[4]   R. L. Yadav and A. W. Patwardhan, "Design Aspects of Pulsed Sieve Plate Columns," *Chem. Eng. J.*, vol. 138, no. 1–3, pp. 389–415, 2008.

[5]   R. L. Yadav and A. W. Patwardhan, "CFD Modeling of Sieve and Pulsed-Sieve Plate Extraction Columns," *Chem. Eng. Res. Des.*, vol. 87, no. 1, pp. 25–35, 2009.

[6]   G. U. Din, I. R. Chughtai, M. H. Inayat, I. H. Khan, and N. K. Qazi, "Modeling of a Two-Phase Countercurrent Pulsed Sieve Plate Extraction Column - A Hybrid CFD and Radiotracer RTD Analysis Approach," *Sep. Purif. Technol.*, vol. 73, no. 2, pp. 302–309, 2010.

[7]   N. S. Kolhe *et al.*, "CFD and Experimental Studies of Single-Phase Axial Dispersion Coefficient in Pulsed Sieve Plate Column," *Chem. Eng. Res. Des.*, vol. 89, no. 10, pp. 1909–1918, 2011.

[8]   K. L. Nash and G. J. Lumetta, *Advanced Separation Techniques for Nuclear Fuel Reprocessing and Radioactive Waste Treatment*. Cambridge: Elsevier Science, 2011.

[9]   D. H. Logsdail and M. J. Slater, "Pulsed Perforated-Plate Columns," in *Handbook of Solvent Extraction*, T. C. Lo, M. H. I. Baird, and C. Hanson, Eds. New York: Wiley, 1983, pp. 355–372.

[10]   Z. Khatir, B. C. Hanson, M. Fairweather, and P. J. Heggs, "High-fidelity CFD simulations of pulsed sieve-plate extraction columns," in *ETMM11*, 2016.

[11]   K. Escoe, *Piping and Pipelines Assessment Guide*. Burlington: Elsevier Science, 2006.

[12]   J. J. McKetta, *Encyclopedia of Chemical Processing and Design: Volume 65 -- Waste: Nuclear Reprocessing and Treatment Technologies to Wastewater Treatment: Multilateral Approach*. Boca Raton: Taylor & Francis, 1998.

[13] Perry, R. H., & Green, D. W. (2008). *Perry's chemical engineers' handbook. New York: McGraw-Hill.*

[14] W. R. Gambill, "How to estimate mixtures viscosities," *Chem. Eng.*, vol. 66, no. 5, pp. 151–152, 1959.

[15] T. Mukha and M. Liefvendahl, "Large-Eddy Simulation of Turbulent Channel Flow," Uppsala, 2015.

[16] C. Meneveau, T. S. Lund, and W. H. Cabot, "A Lagrangian dynamic subgrid-scale model of turbulence," *J. Fluid Mech.*, vol. 319, pp. 353–385, 1996.

[17] OpenCFD Ltd, "OpenFOAM User Guide," OpenCFD Ltd (ESI Group), Bracknell, 2016.

[18] R. Stoll and F. Porté-Agel, "Dynamic Subgrid-Scale Models for Momentum and Scalar Fluxes in Large-Eddy Simulations of Neutrally Stratified Atmospheric Boundary Layers Over Heterogeneous Terrain," *Water Resour. Res.*, vol. 42, no. 1, pp. 1–18, 2006.

[19] G. H. Yeoh and J. Tu, "Computational techniques for multiphase flows." Butterworth-Heinemann, Oxford;Burlington, MA;, 2009.

[20] J. D. Thornton, "LIQUID-LIQUID EXTRACTIIN PART XIII : THE EFFECT OF PULSE WAVE-FORM AND PLATE GEOMETRY IN THE PERFFRMANCE AND THROUGHPUT F A PULSED COLUMNS," *Transations Inst. Chem. Eng.*, vol. 35, pp. 316–330, 1957.

[21] M. M. Hafez and M. H. I. Baird, "Power consumption in a reciprocating plate extraction column," *Trans. Inst. Chem. Eng*, vol. 56, pp. 229–238, 1978.

[22] P. J. Cullen, *Food Mixing: Principles and Applications*. Wiley, 2009.

ACKOWLEDGEMENTS